

Supporting Information

Electrochemical formation and dissolution of an Iodine-Halide coordination solid complex in a nano-confined space

*Jaehyun Jeon,^a Jiseon Hwang,^{a,b} Jung Hoon Yang,^c Jinho Chang^{*a,d}*

^aDepartment of Chemistry and Research Institute for Convergence of Basic Science, Hanyang University, Seoul 04763, Republic of Korea

^bCurrent address: Department of Chemistry and Biochemistry, Ohio State University, Columbus, Ohio 43210 USA

^cKorea Institute of Energy Research (KIER), Daejeon 34129, Republic of Korea

^dDepartment of HY-KIST Bio-convergence, Hanyang University, Seoul 04763, Republic of Korea

Contents

Detailed description for equation 4	S-5
Estimation of the specific cell capacitance (SC_{cell}), energy density (ED), and power density (PD) in (-)micro-C NaI(aq) with/without NaBr(aq) micro-C(+)	S-6
Estimation of C_{ZIRB} from (-)Zn 0.2 M ZnSO ₄ + 10 mM NaI with/without 5 mM NaBr micro-C(+)	S-6
Fig. S1	S-7
FE-SEM images of (a) micro-C and (b) PG, (c) N ₂ ADS and DES and (d) the corresponding pore size distribution in micro-C.	
Fig. S2	S-8
Potential vs. pH for iodine/H ₂ O system in an aqueous solution at 25 °C. Reprinted from Frackowiak et al. ^[2] Copyright (2014) with permission from Elsevier.	
Fig. S3	S-9
CVs from (a) (-)micro-C 0.1 M NaI PG(+) and (b) (-)micro-C 0.05 M NaBr PG(+) at 2 mV/s.	
Fig. S4	S-10
The integrated area to estimate Q_{Ox} and Q_{Red} from CVs on a micro-C measured in (-)micro-C 0.1 M NaI(aq) (a) without/(b) with 0.05 M NaBr(aq) micro-C(+), respectively.	
Fig. S5	S-11
2D axial symmetric domain of the simulation for the theoretical model.	
Fig. S6	S-12
(a, c) Simulated steady-state voltammograms associated with electro-oxidation of I ⁻ in a solution containing (a) I ⁻ only, and (c) I ⁻ and Br ⁻ . (b, d) Corresponding concentration profiles of each species vs. η at the electrode surface in the voltammogram from a solution with (b) I ⁻ only and (d) I ⁻ and Br ⁻ .	
Fig. S7	S-13
The reproducibility test of E_{cell} (black), E_+ (red), and E_- (blue)-profiles vs. t at 0.5 A g ⁻¹ from (a) (-)micro-C 0.5 M NaI micro-C(+) and (b) (-)micro-C 0.5 M NaI + 0.4 M NaBr micro-C(+).	
Fig. S8	S-14
E_{cell} (black), E_+ (red), and E_- (blue)-profiles as a function of t at constantly applied 0.5 A g ⁻¹ to the two electrochemical cells configured as (a) micro-C 0.5 M NaI PG and (b) micro-C 0.5 M NaI + 0.4 M NaBr PG, respectively.	
Fig. S9	S-15

(a) The charge/discharge profiles vs. t and (b) SC_{cell} at 0.5 A g^{-1} from the symmetric cells containing 0.5 M NaI with different concentration of Br^- .

Fig. S10S-16

E_{cell} vs. t curves at different current densities from (-)micro-C| 0.5 M NaI |micro-C(+) (black), (-)micro-C| $0.5 \text{ M NaI} + 0.4 \text{ M NaBr}$ |micro-C(+) (blue), and (-)micro-C| $0.5 \text{ M NaI} + 0.4 \text{ M NaNO}_3$ |micro-C(+) (red).

Fig. S11S-17

Cycle stability of (-)micro-C| $0.5 \text{ M NaI} + 0.4 \text{ M NaBr}$ |micro-C(+) at 4 A g^{-1} .

Fig. S12S-18

Deconvoluted high-resolution Na 2s XPS spectrum from micro-C serving as the positive electrode after charging to $E_{\text{cell}} = 1.3 \text{ V}$ at 0.5 A g^{-1} from (-)micro-C| 0.5 M NaI |micro-C(+).

Fig. S13S-19

SEM images and corresponding EDS elemental mapping from micro-C serving as positive electrodes in (-)micro-C| 0.5 M NaI |micro-C(+) cell after charging to $E_{\text{cell}} = 1.3 \text{ V}$. The micro-C were analyzed after rinsing with DI water.

Fig. S14S-20

(a) Raman spectra and (b) a deconvoluted high-resolution I 3d XPS spectrum from micro-C serving as positive electrodes after charging to $E_{\text{cell}} = 1.3 \text{ V}$ at 0.5 A g^{-1} from (-)micro-C| $0.5 \text{ M NaI} + 0.4 \text{ M NaBr}$ |micro-C(+).

Fig. S15S-21

The SEM images and corresponding EDS elemental mapping from micro-C serving as positive electrodes in (-)micro-C| 0.5 M NaI with 0.4 M NaBr |micro-C(+) cell after charging at 0.5 A g^{-1} to $E_{\text{cell}} = 1.3 \text{ V}$. The micro-C were analyzed after rinsing with DI water.

Fig. S16S-22

E_{cell} vs. t curves in the ZIRB containing 10 mM NaI with (red)/ without (black) 5 mM NaBr at (a) 0.3 A g^{-1} and (b) 0.015 A g^{-1} .

Fig. S17S-23

The reproducibility test of E_{cell} vs. C_{ZIRB} curves in a model ZIRB containing 10 mM NaI with (red)/without (black) 5 mM NaBr at (a) 0.3 A g^{-1} and (b) 0.015 A g^{-1} .

Fig. S18S-24

E_{cell} vs. C_{ZIRB} curves in model ZIRBs at various current densities from (-)Zn| $0.2 \text{ M ZnSO}_4(\text{aq}) + 10 \text{ mM NaI}(\text{aq})$ |micro-C(+) (black), (-)Zn| $0.2 \text{ M ZnSO}_4(\text{aq}) + 10 \text{ mM NaI}(\text{aq}) + 5 \text{ mM NaBr}(\text{aq})$ |micro-C(+) (blue), and (-)Zn| $0.2 \text{ M ZnSO}_4(\text{aq}) + 10 \text{ mM NaI}(\text{aq}) + 5 \text{ mM NaNO}_3(\text{aq})$ |micro-C(+) (red), respectively.

Table S1.	S-25
Reactions and corresponding parameters for a simulation without Br ⁻ , with results displayed as simulated voltammograms and corresponding concentration profiles in Figure 2b-c and Figure S6a-b, respectively.	
Table S2.	S-26
Reactions and corresponding parameters for a simulation with Br ⁻ , with results are displayed as simulated voltammograms and the corresponding concentration profiles in Figure 2d-e and Figure S6c-d, respectively.	
Table S3.	S-28
ED at a specific PD from the electrochemical capacitors operated in an aqueous solution with various redox active species.	
Abbreviations	S-29
References	S-31

Detailed description for equation 4

For the $I_2(aq)_{bulk}/I^-(aq)$ redox reaction in reaction S1, the half-redox potential, $E_{I_2(aq)_{bulk}/I^-(aq)}$ can be expressed as a Nernst equation:



$$E_{I_2(aq)_{bulk}/I^-(aq)} = E_{I_2(aq)_{bulk}/I^-(aq)}^\circ - \frac{RT}{n_e F} \ln \left(\frac{C_{I^-(aq)}^2}{C_{I_2(aq)_{bulk}}} \right) \quad (S2)$$

where n_e is the number of electrons in the redox reaction, which is 2. The half-redox potential of the $I_2(aq)_{pore}/I^-(aq)$ redox reaction (reaction S3), $E_{I_2(aq)_{pore}/I^-(aq)}$, can also be expressed as:



$$E_{I_2(aq)_{pore}/I^-(aq)} = E_{I_2(aq)_{pore}/I^-(aq)}^\circ - \frac{RT}{2F} \ln \left(\frac{C_{I^-(aq)}^2}{C_{I_2(aq)_{pore}}} \right) \quad (S4)$$

At equilibrium, $E_{I_2(aq)_{bulk}/I^-(aq)}$ is the same as $E_{I_2(aq)_{pore}/I^-(aq)}$. Therefore, the difference between the two half-redox potentials, ΔE , can be expressed as:

$$\Delta E = \left\{ E_{I_2(aq)_{bulk}/I^-(aq)}^\circ - E_{I_2(aq)_{pore}/I^-(aq)}^\circ \right\} - \frac{RT}{2F} \ln \left(\frac{C_{I_2(aq)_{pore}}}{C_{I_2(aq)_{bulk}}} \right) \quad (S5)$$

Because $C_{I_2(aq)_{pore}}/C_{I_2(aq)_{bulk}}$ at equilibrium is K_{stab} , we can derive equation 4 in the article from equation S5.

Estimation of specific cell capacitance (SC_{cell}), energy density (ED), and power density (PD) in (-)micro-C|NaI(aq) with/without NaBr(aq)|micro-C(+)

In micro-C|NaI(aq) with/without NaBr(aq)|micro-C, SC_{cell} ($F\ g^{-1}$) was estimated from charge/discharge curves using equation S6:^[1]

$$SC_{spec, cell} = i \cdot \Delta t / (\Delta V \cdot m) \quad (S6)$$

where ΔV is the driven cell potential, i is the applied current at charge and discharge, Δt is the time during charge and discharge, and m is the mass of the total micro-C in both the positive and negative electrodes of the symmetric cell.

The ED (Wh/kg) and PD (W/kg) of the cell were estimated from discharge curves using:^[2]

$$ED = \frac{1}{2} SC_{cell} \Delta V^2 \quad (S7)$$

$$PD = ED / \Delta t \quad (S8)$$

Estimation of C_{ZIRB} from (-)Zn|0.2 M ZnSO₄ + 10 mM NaI with/without 5 mM NaBr|micro-C(+)

The E_{cell} vs. capacity curves in Figure 4 were obtained from the E_{cell} vs. t curves at constantly applied currents in Figure S11, and the specific capacity of the corresponding electrochemical cells was estimated by:

$$C_{ZIRB} = i \cdot \Delta t / m \quad (S9)$$

where m is the mass of micro-C in the cell.

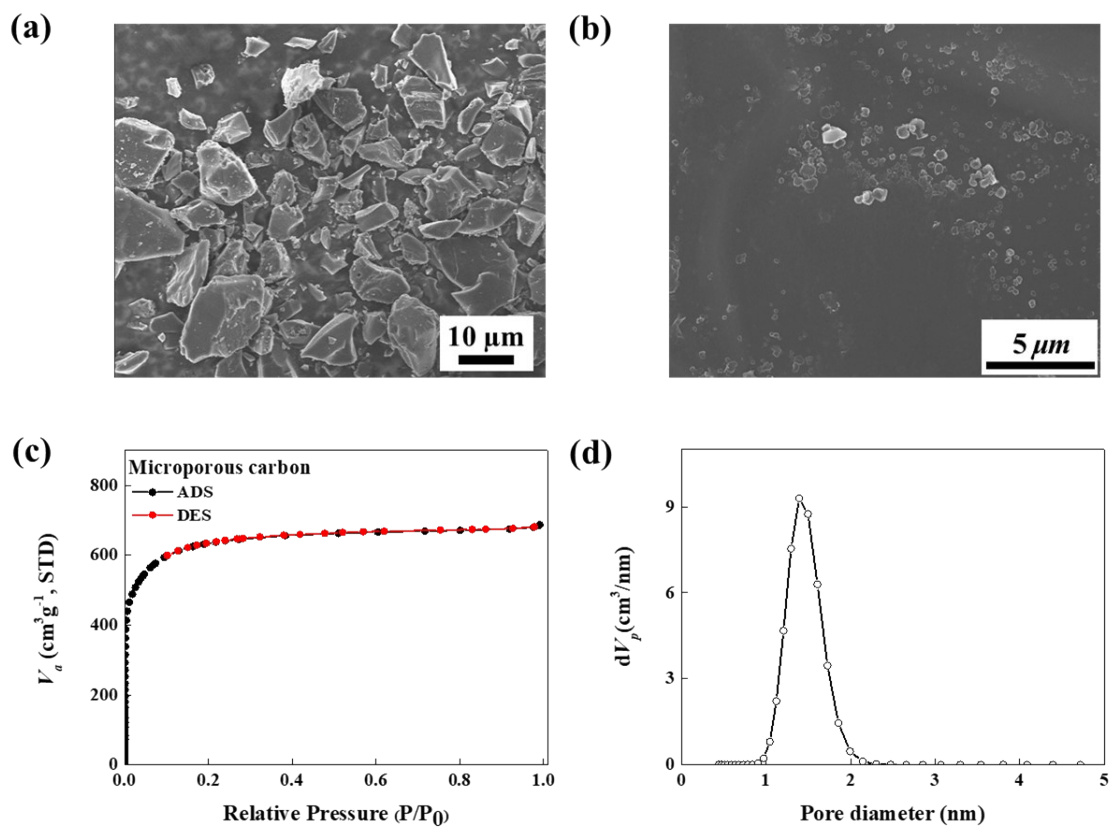


Fig. S1 The FE-SEM images of (a) micro-C and (b) PG, (c) N₂ ADS and DES and (d) the corresponding pore-size distribution in micro-C.

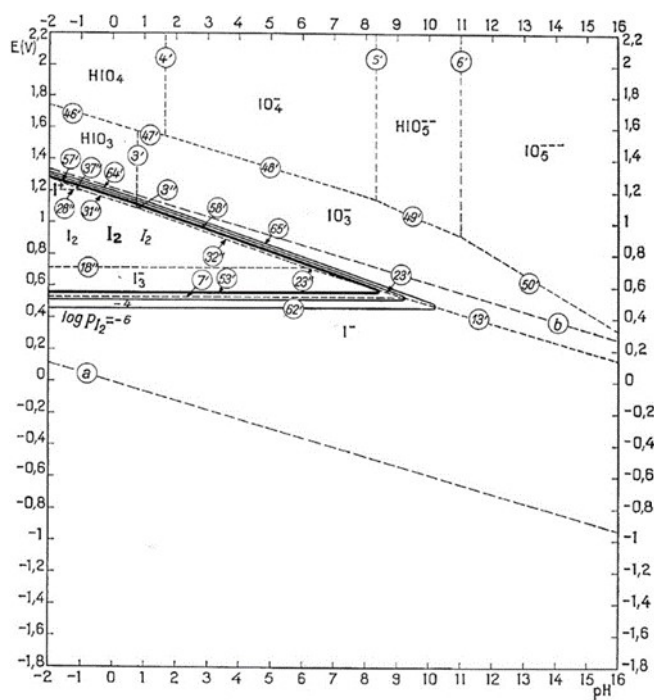


Fig. S2 Potential vs. pH for an iodine/H₂O system in an aqueous solution at 25 °C. Reprinted from Frackowiak et al.^[2] Copyright (2014) with permission from Elsevier.

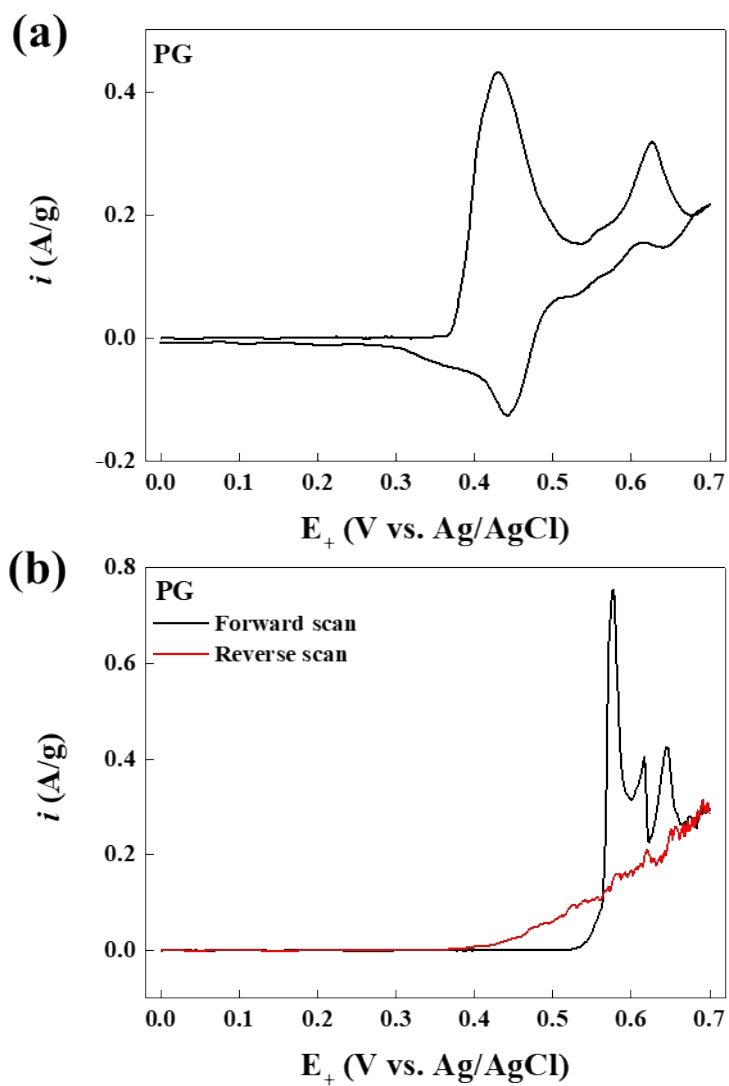


Fig. S3 CVs from (a) (-)micro-C|0.1 M NaCl|PG(+) and (b) (-)micro-C|0.05 M NaBr|PG(+) at 2 mV s⁻¹.

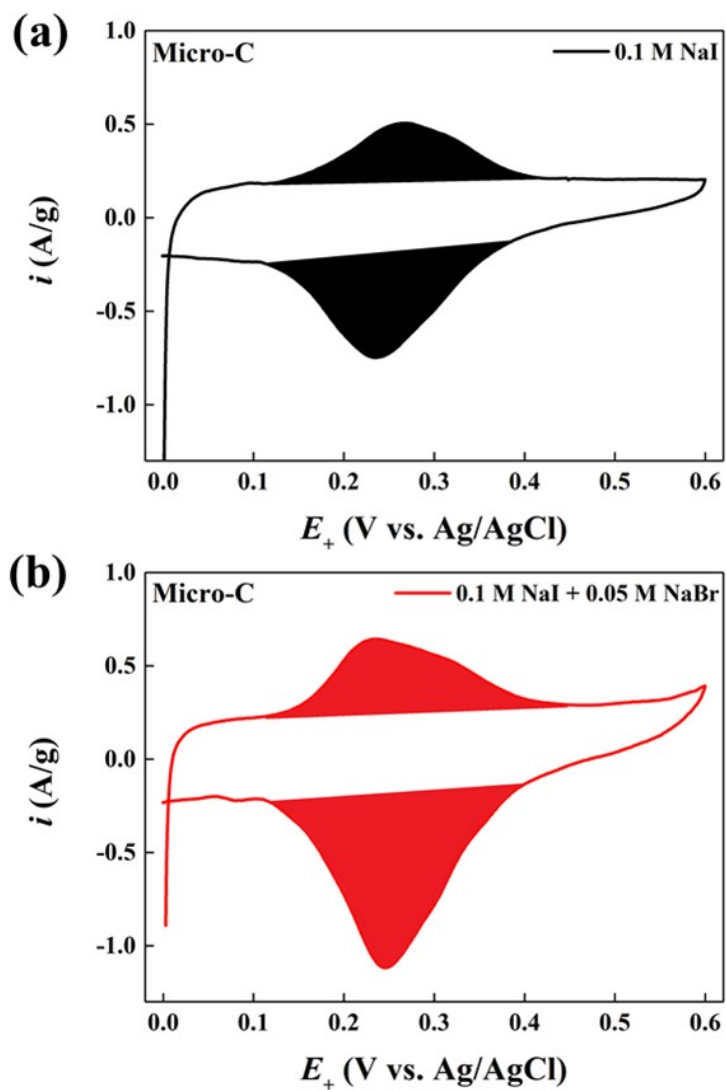


Fig. S4 The integrated area to estimate Q_{Ox} and Q_{Red} from CVs on a micro-C measured in (-)micro-C|0.1 M NaI(aq) (a) without/(b) with 0.05 M NaBr(aq)|micro-C(+), respectively.

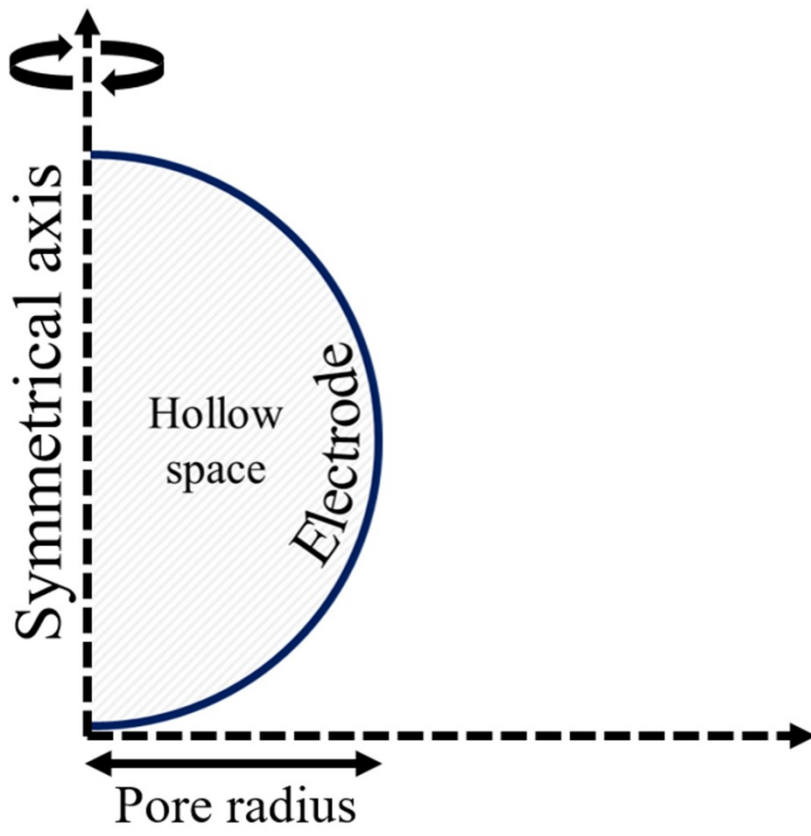


Fig. S5 2D axial symmetric domain of the simulation for the theoretical model.

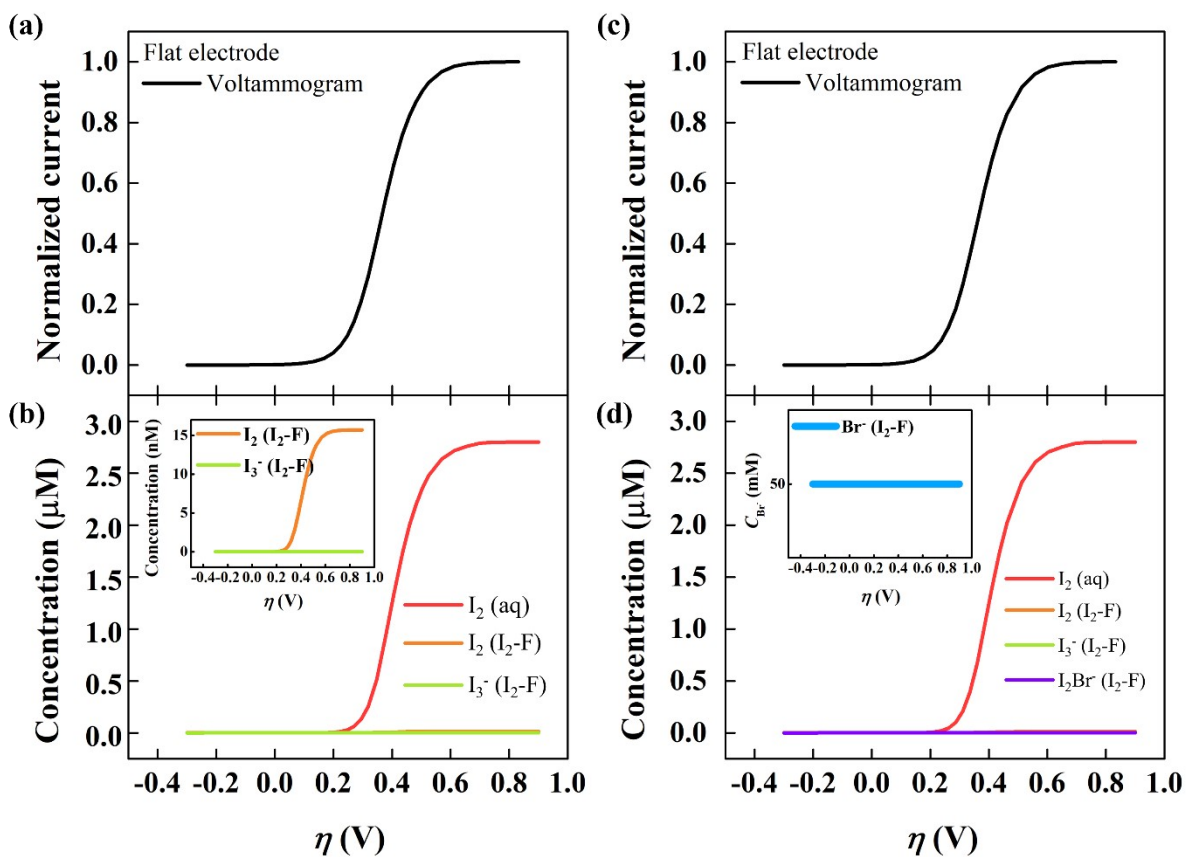


Fig. S6 (a, c) Simulated steady-state voltammograms associated with electro-oxidation of I^- in a solution containing (a) I^- only, and (c) I^- and Br^- . (b, d) Corresponding concentration profiles of each species vs. η at the electrode surface in the voltammogram from a solution with (b) I^- only and (d) I^- and Br^- .

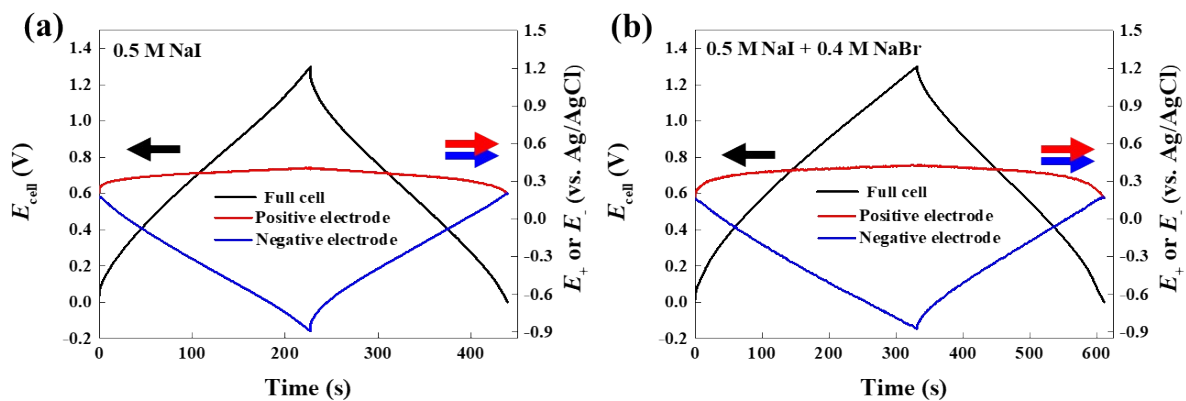


Fig. S7 The reproducibility test of E_{cell} (black), E_+ (red), and E_- (blue)-profiles vs. t at 0.5 A g^{-1} from (a) (-)micro-C|0.5 M NaI|micro-C(+) and (b) (-)micro-C|0.5 M NaI + 0.4 M NaBr|micro-C(+).

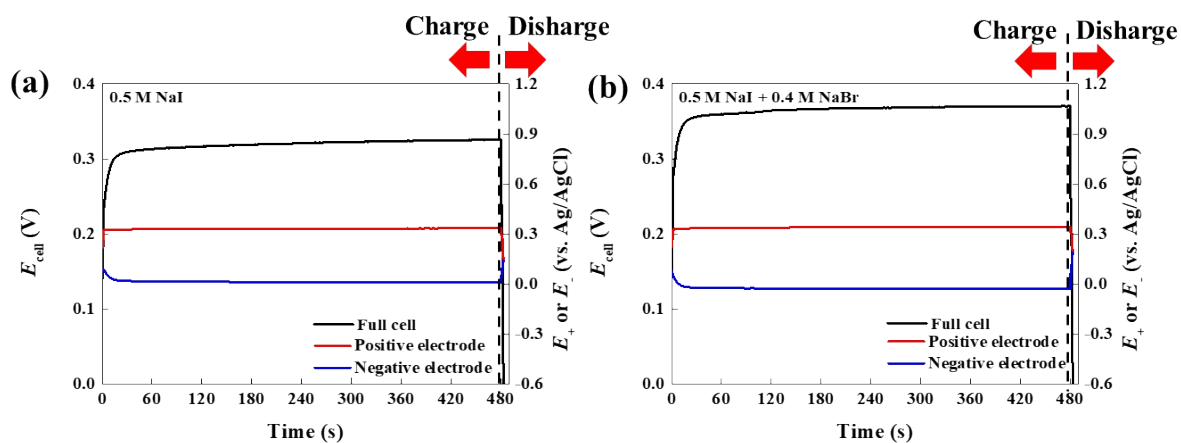


Fig. S8 E_{cell} (black), E_+ (red), and E_- (blue)-profiles as a function of t at constantly applied 0.5 A g^{-1} to the two electrochemical cells configured as (a) micro-C|0.5 M NaI|PG and (b) micro-C|0.5 M NaI + 0.4 M NaBr|PG, respectively.

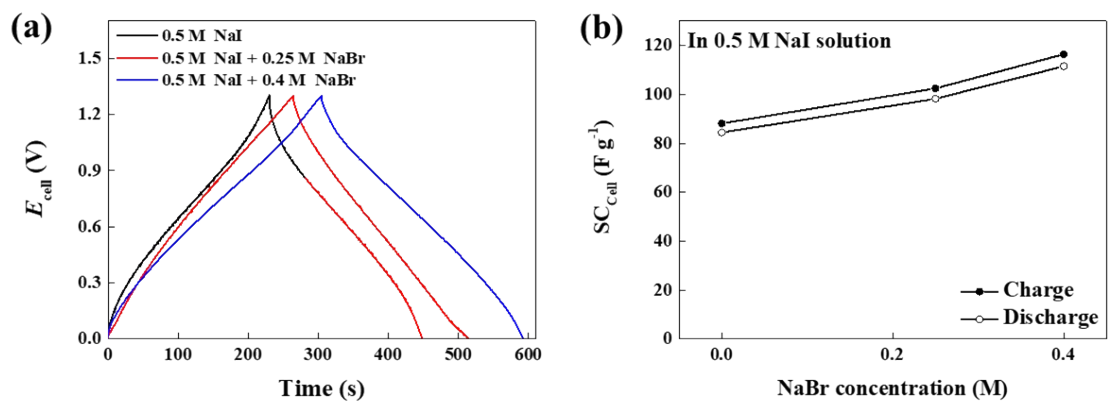


Fig. S9 (a) The charge/discharge profiles vs. t and (b) SC_{cell} at 0.5 A g^{-1} from the symmetric cells containing 0.5 M NaI with different concentration of Br^- .

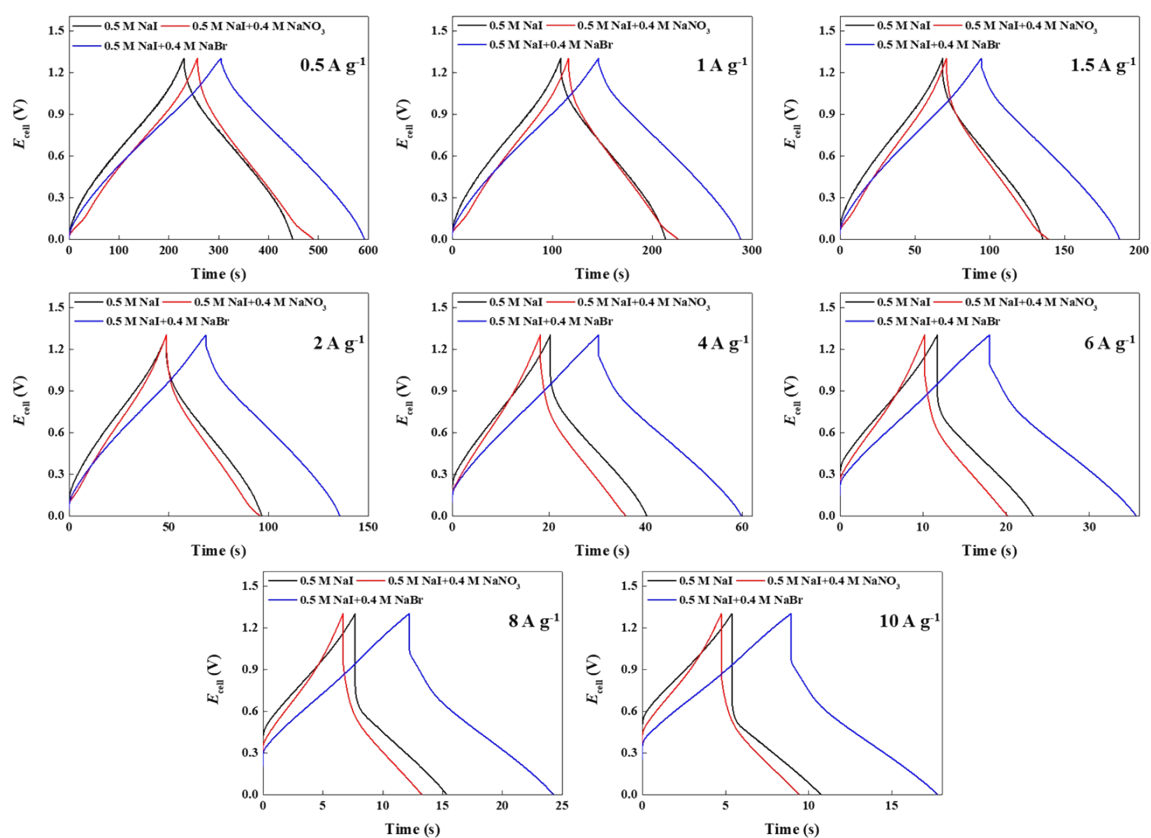


Fig. S10 E_{cell} vs. t curves at different current densities from (-)micro-C|0.5 M NaI|micro-C(+) (black), (-)micro-C|0.5 M NaI + 0.4 M NaBr|micro-C(+) (blue), and (-)micro-C|0.5 M NaI + 0.4 M NaNO₃|micro-C(+) (red).

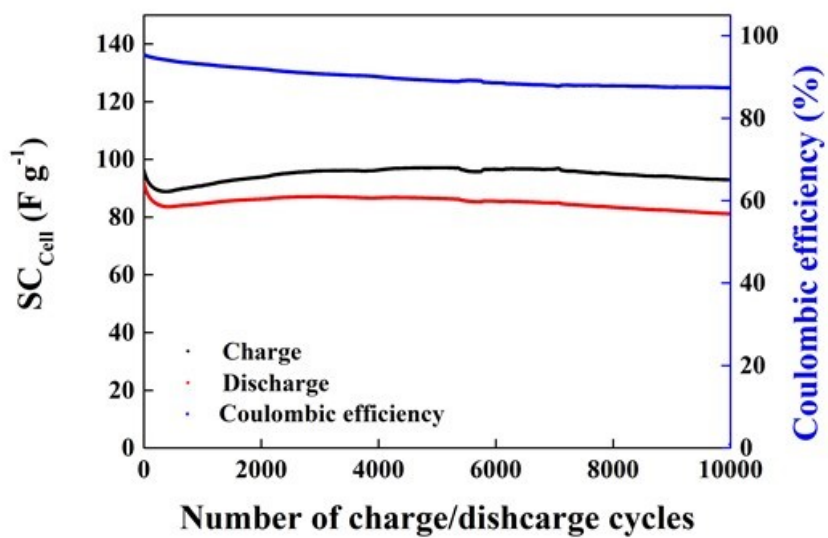


Fig. S11 Cycle stability of (-)micro-C|0.5 M NaI + 0.4 M NaBr|micro-C(+) at 4 A g⁻¹.

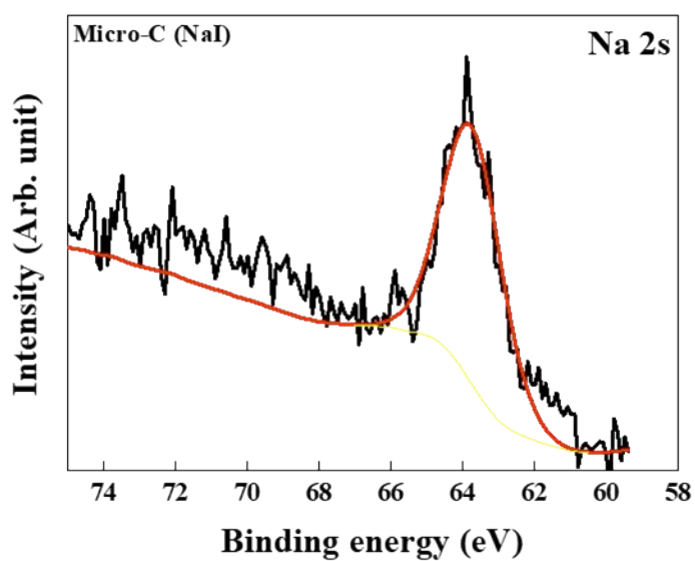
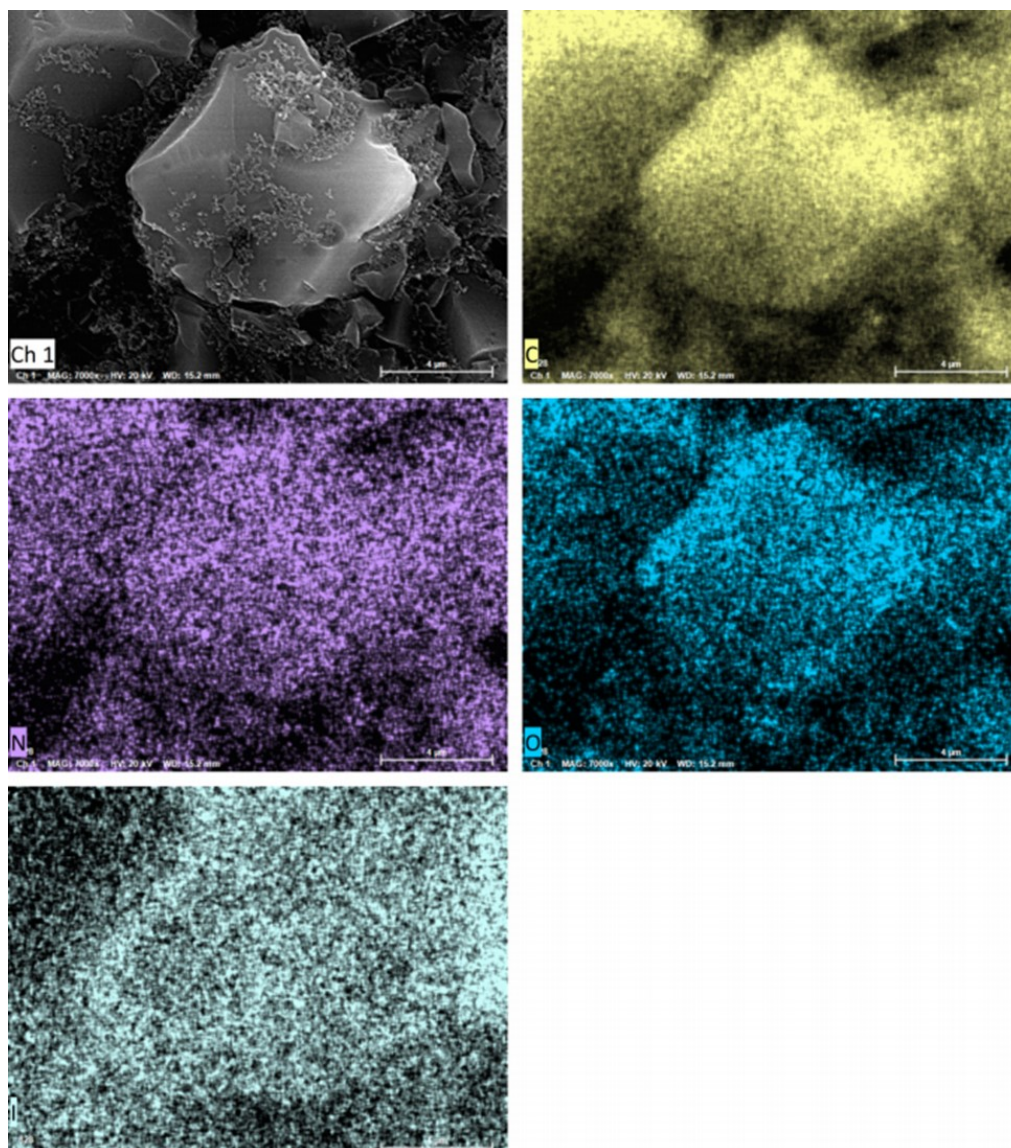


Fig. S12 Deconvoluted high-resolution Na 2s XPS spectrum from micro-C serving as the positive electrode after charging to $E_{\text{cell}} = 1.3$ V at 0.5 A g^{-1} from (-)micro-C|0.5 M NaI|micro-C(+).



Element	At. No.	Netto	Mass [%]	Mass Norm. [%]	Atom [%]	abs. error [%] (3 sigma)	rel. error [%] (3 sigma)
C	6	1120130	62.54	63.08	84.33	19.57	31.29
N	7	31650	8.79	8.87	10.17	3.31	37.62
O	8	21097	2.21	2.23	2.24	0.96	43.46
I	53	979952	25.61	25.83	3.27	2.24	8.75
		Sum	99.15	100.00	100.00		

Fig. S13 SEM images and corresponding EDS elemental mapping from micro-C serving as positive electrodes in (-)micro-C|0.5 M NaI|micro-C(+) cell after charging to $E_{\text{cell}} = 1.3$ V.

The micro-C were analyzed after rinsing with DI water.

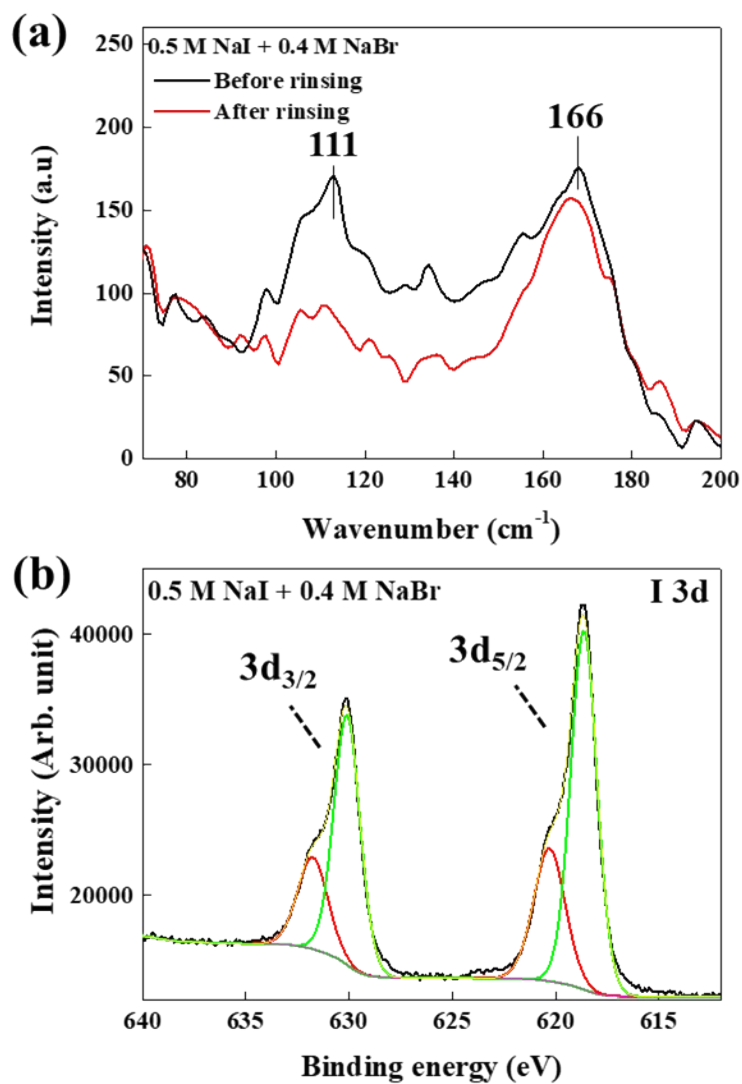
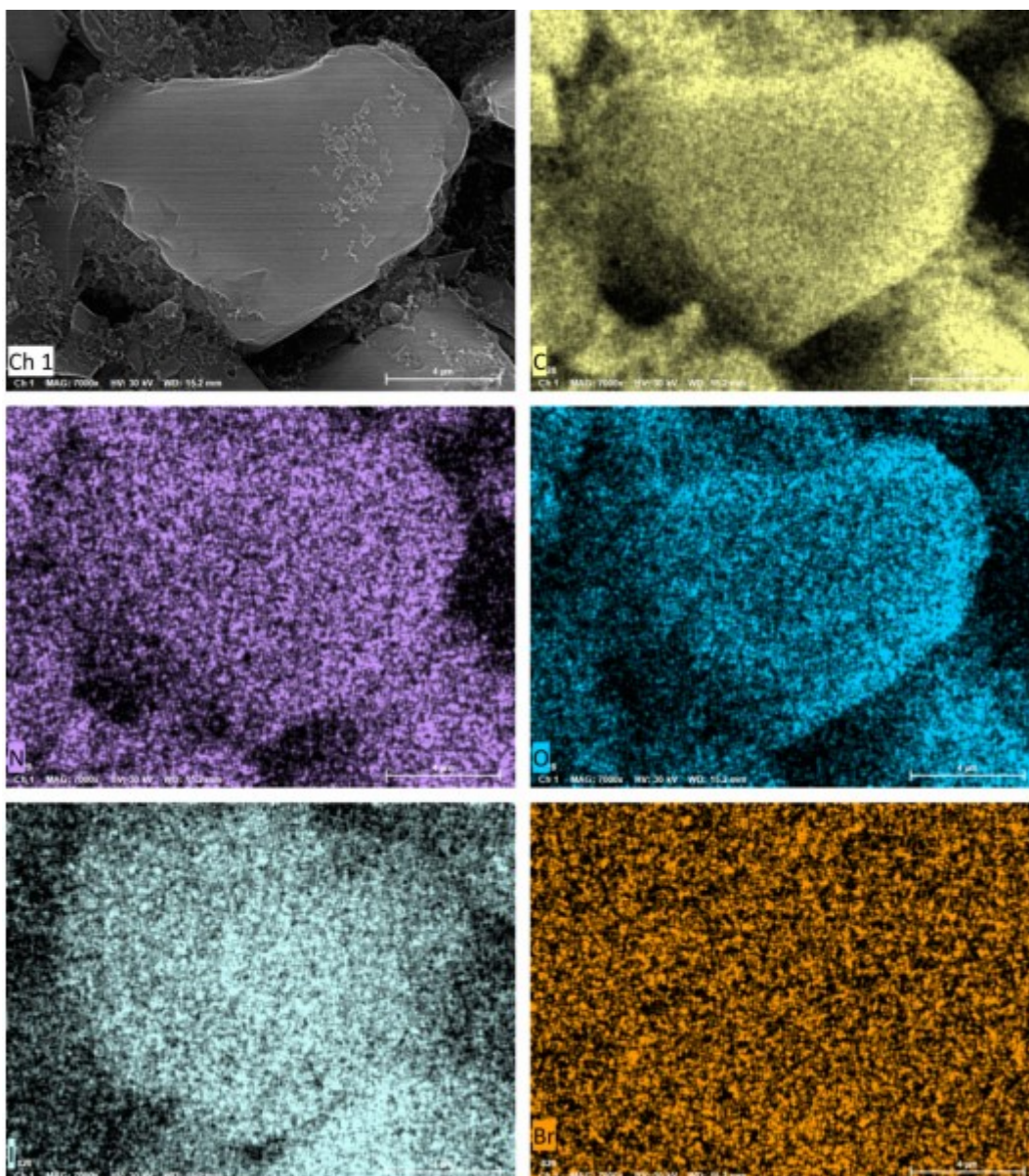


Fig. S14 (a) Raman spectra and (b) a deconvoluted high-resolution I 3d XPS spectrum from micro-C serving as positive electrodes after charging to $E_{\text{cell}} = 1.3 \text{ V}$ at 0.5 A g^{-1} from (-)micro-C|0.5 M NaI + 0.4 M NaBr|micro-C(+).



Map

Element	At. No.	Netto	Mass [%]	Mass Norm. [%]	Atom [%]	abs. error [%] (3 sigma)	rel. error [%] (3 sigma)
C	6	1197266	54.29	55.10	82.14	16.98	31.27
N	7	45228	8.29	8.41	10.75	3.03	36.60
O	8	27711	1.98	2.01	2.25	0.86	43.25
I	53	4634944	33.97	34.47	4.86	2.94	8.65
Br	35	0	0.00	0.00	0.00	0.00	1.33
		Sum	98.52	100.00	100.00		

Fig. S15 The SEM images and corresponding EDS elemental mapping from micro-C serving as positive electrodes in (-)micro-C|0.5 M NaI with 0.4 M NaBr|micro-C(+) cell after charging at 0.5 A g⁻¹ to $E_{\text{cell}} = 1.3$ V. The micro-C were analyzed after rinsing with DI water.

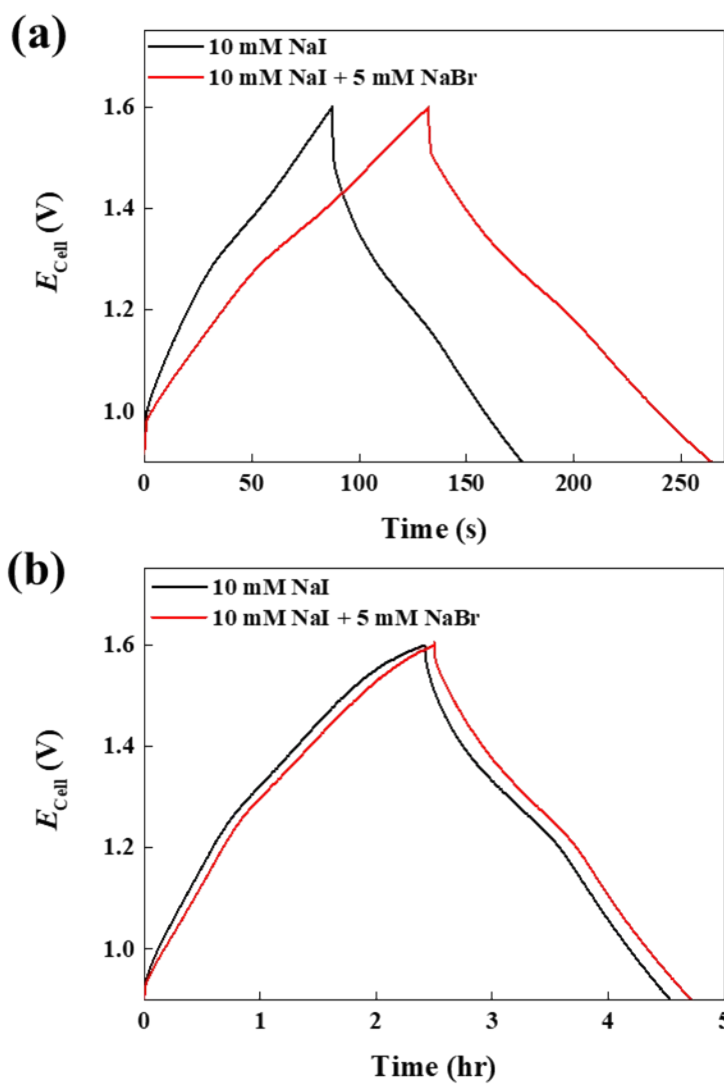


Fig. S16 E_{cell} vs. t curves in the ZIRB containing 10 mM NaI with (red)/ without (black) 5mM NaBr at (a) 0.3 A g^{-1} and (b) 0.015 A g^{-1} .

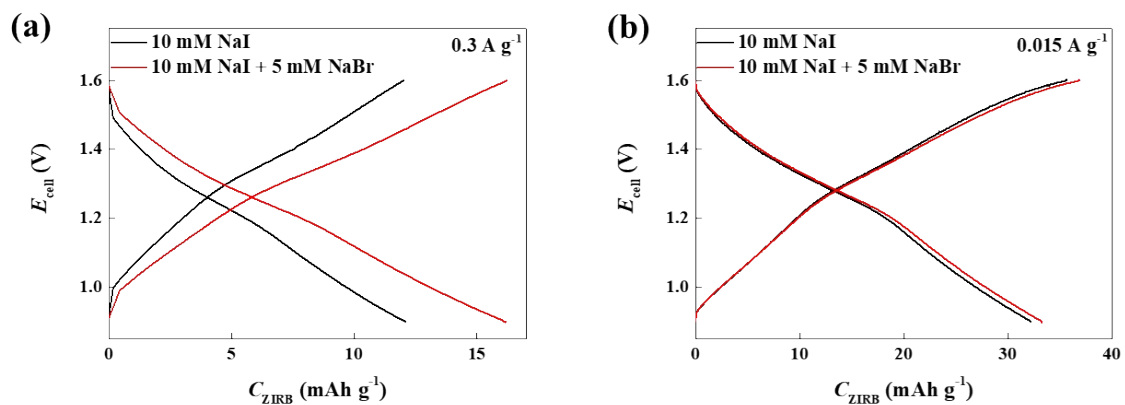


Fig. S17 The reproducibility test of E_{cell} vs. C_{ZIRB} curves in a model ZIRB containing 10 mM NaI with (red)/without (black) 5 mM NaBr at (a) 0.3 A g^{-1} and (b) 0.015 A g^{-1} .

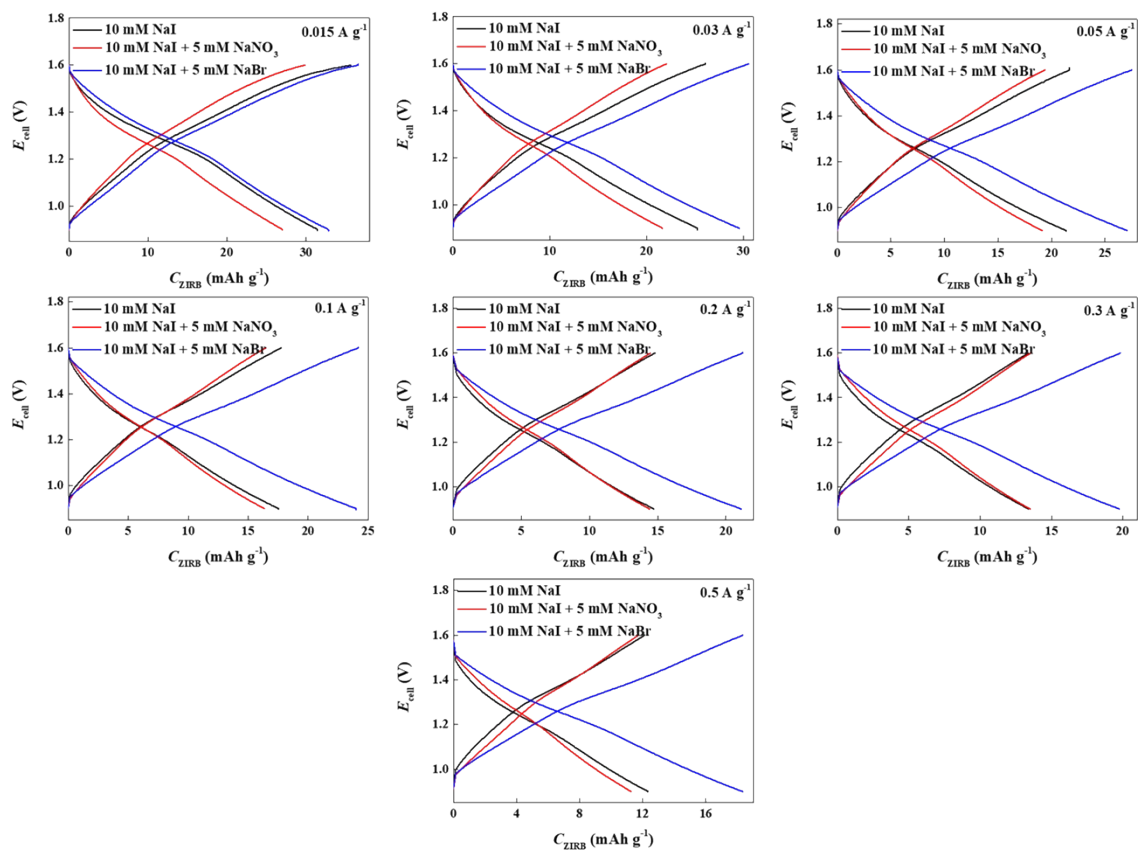


Fig. S18 E_{cell} vs. C_{ZIRB} curves in model ZIRBs at various current densities from (-)Zn|0.2 M $\text{ZnSO}_4(\text{aq}) + 10 \text{ mM NaI}(\text{aq})$ |micro-C(+) (black), (-)Zn|0.2 M $\text{ZnSO}_4(\text{aq}) + 10 \text{ mM NaI}(\text{aq}) + 5 \text{ mM NaBr}(\text{aq})$ |micro-C(+) (blue), and (-)Zn|0.2 M $\text{ZnSO}_4(\text{aq}) + 10 \text{ mM NaI}(\text{aq}) + 5 \text{ mM NaNO}_3(\text{aq})$ |micro-C(+) (red), respectively.

Table S1. Reactions and corresponding parameters for a simulation without Br⁻, with results displayed as simulated voltammograms and corresponding concentration profiles in Figure 2b-c and Figure S6a-b, respectively.

Reactions	Parameters
$I \cdot + e^- \rightleftharpoons I(aq)$	$E_{eq} = 0.3 \text{ V}$, $k^0 = 0.1 \text{ cm/s}$, $\alpha = 0.5$
$2I \cdot \rightleftharpoons I_2(aq)$	$K_{eq,(6)} = 200$
$I_2(aq) \rightleftharpoons I_2(I_2-F)$	$K_{eq,(7)} = 1000$
$I(I_2-F) + I_2(I_2-F) \rightleftharpoons I_3^-(I_2-F)$	$K_{eq,(8)} = 724$
Relevant time-dependent diffusion equations	
(1) $\frac{\partial C_{I \cdot}}{\partial t} = D_{I \cdot} \left[\frac{\partial^2 C_{I \cdot}}{\partial r^2} + \frac{2}{r} \frac{\partial C_{I \cdot}}{\partial r} \right] - 2k_{f,eq,(6)} C_{I \cdot}^2 + 2k_{b,eq,(6)} C_{I_2(aq)}$	
(2) $\frac{\partial C_{I^-(I_2-F)}}{\partial t} = D_{I^-(I_2-F)} \left[\frac{\partial^2 C_{I^-(I_2-F)}}{\partial r^2} + \frac{2}{r} \frac{\partial C_{I^-(I_2-F)}}{\partial r} \right] - k_{f,eq,(8)} C_{I_2(I_2-F)} C_{I^-(I_2-F)} + k_{b,eq,(8)} C_{I_3^-(I_2-F)}$	
(3) $\frac{\partial C_{I_2(aq)}}{\partial t} = D_{I_2(aq)} \left[\frac{\partial^2 C_{I_2(aq)}}{\partial r^2} + \frac{2}{r} \frac{\partial C_{I_2(aq)}}{\partial r} \right] + k_{f,eq,(6)} C_{I \cdot}^2 - k_{b,eq,(6)} C_{I_2(aq)}$	
(4) $\frac{\partial C_{I_2(I_2-F)}}{\partial t} = D_{I_2(I_2-F)} \left[\frac{\partial^2 C_{I_2(I_2-F)}}{\partial r^2} + \frac{2}{r} \frac{\partial C_{I_2(I_2-F)}}{\partial r} \right] + k_{f,eq,(7)} C_{I_2(aq)} - k_{b,eq,(7)} C_{I_2(I_2-F)} + k_{b,eq,(8)} C_{I_3^-(I_2-F)}$	
(5) $\frac{\partial C_{I_3^-(I_2-F)}}{\partial t} = D_{I_3^-(I_2-F)} \left[\frac{\partial^2 C_{I_3^-(I_2-F)}}{\partial r^2} + \frac{2}{r} \frac{\partial C_{I_3^-(I_2-F)}}{\partial r} \right] + k_{f,eq,(8)} C_{I_2(I_2-F)} C_{I^-(I_2-F)} - k_{b,eq,(8)} C_{I_3^-(I_2-F)}$	
Initial condition, completing the definition of the problem	
$t = 0$, $C_{I^-(I_2-F)} = C_{I_2(aq)} = C_{I_2(I_2-F)} = C_{I_3^-(I_2-F)} = 0$, $C_{I \cdot} = 100 \text{ mM}$	
$D_{I \cdot} = D_{I^-(I_2-F)} = D_{I_3^-(I_2-F)} = 1.47 \times 10^{-5}$, $D_{I_2(I_2-F)} = 1.72 \times 10^{-5}$	
$D_{I_2(aq)} = 3.00 \times 10^{-8} \text{ cm s}^{-1}$	

Table S2. Reactions and the Corresponding parameters for a simulation with Br⁻, with results displayed as simulated voltammograms and corresponding concentration profiles in Figure 2d-e and Figure S6c-d, respectively.

Reactions	Parameters
$I \cdot + e^- \rightleftharpoons I^-(aq)$	$E_{eq} = 0.3 \text{ V}, k^0 = 0.1 \text{ cm/s}, \alpha = 0.5$
$2I \cdot \rightleftharpoons I_2(aq)$	$K_{eq,(6)} = 200$
$I_2(aq) \rightleftharpoons I_2(I_2-F)$	$K_{eq,(7)} = 1000$
$I_2(I_2-F) + I(I_2-F) \rightleftharpoons I_3^-(I_2-F)$	$K_{eq,(8)} = 724$
$I_2(I_2-F) + Br^-(I_2-F) \rightleftharpoons I_2Br^-(I_2-F)$	$K_{eq,(9)} = 12$
Relevant time-dependent diffusion equations	
(1) $\frac{\partial C_{I \cdot}}{\partial t} = D_{I \cdot} \left[\frac{\partial^2 C_{I \cdot}}{\partial r^2} + \frac{2}{r} \frac{\partial C_{I \cdot}}{\partial r} \right] - 2k_{f,eq,(6)} C_{I \cdot}^2 + 2k_{b,eq,(6)} C_{I_2(aq)}$	
(2) $\frac{\partial C_{I^-(I_2-F)}}{\partial t} = D_{I^-(I_2-F)} \left[\frac{\partial^2 C_{I^-(I_2-F)}}{\partial r^2} + \frac{2}{r} \frac{\partial C_{I^-(I_2-F)}}{\partial r} \right] - k_{f,eq,(8)} C_{I_2(I_2-F)} C_{I^-(I_2-F)} + k_{b,eq,(8)} C_{I_3^-(I_2-F)}$	
(3) $\frac{\partial C_{I_2(aq)}}{\partial t} = D_{I_2(aq)} \left[\frac{\partial^2 C_{I_2(aq)}}{\partial r^2} + \frac{2}{r} \frac{\partial C_{I_2(aq)}}{\partial r} \right] + k_{f,eq,(6)} C_{I \cdot}^2 - k_{b,eq,(6)} C_{I_2(aq)}$	
(4) $\frac{\partial C_{I_2(I_2-F)}}{\partial t} = D_{I_2(I_2-F)} \left[\frac{\partial^2 C_{I_2(I_2-F)}}{\partial r^2} + \frac{2}{r} \frac{\partial C_{I_2(I_2-F)}}{\partial r} \right] + k_{f,eq,(7)} C_{I_2(aq)} - k_{b,eq,(7)} C_{I_2(I_2-F)} + k_{b,eq,(8)} C_{I_3^-(I_2-F)} - k_{f,eq,(9)} C_{I_2(I_2-F)} C_{Br^-(I_2-F)} + k_{b,eq,(9)} C_{I_2Br^-(I_2-F)}$	
(5) $\frac{\partial C_{I_3^-(I_2-F)}}{\partial t} = D_{I_3^-(I_2-F)} \left[\frac{\partial^2 C_{I_3^-(I_2-F)}}{\partial r^2} + \frac{2}{r} \frac{\partial C_{I_3^-(I_2-F)}}{\partial r} \right] + k_{f,eq,(8)} C_{I_2(I_2-F)} C_{I^-(I_2-F)} - k_{b,eq,(8)} C_{I_3^-(I_2-F)}$	
(6) $\frac{\partial C_{Br^-(I_2-F)}}{\partial t} = D_{Br^-(I_2-F)} \left[\frac{\partial^2 C_{Br^-(I_2-F)}}{\partial r^2} + \frac{2}{r} \frac{\partial C_{Br^-(I_2-F)}}{\partial r} \right] - k_{f,eq,(9)} C_{I_2(I_2-F)}$	

$$(7) \frac{\partial C_{I_2Br^-(I_2-F)}}{\partial t} = D_{I_2Br^-(I_2-F)} \left[\frac{\partial^2 C_{I_2Br^-(I_2-F)}}{\partial r^2} + \frac{2}{r} \frac{\partial C_{I_2Br^-(I_2-F)}}{\partial r} \right] + k_{f,eq,(9)} C_{I_2(I_2-F)} C_{Br^-(I_2-F)} - k_{b,eq,(9)} C_{I_2Br^-(I_2-F)}$$

Initial condition, completing the definition of the problem

$$t = 0, C_{I^-(I_2-F)} = C_{I_2(aq)} = C_{I_2(I_2-F)} = C_{I_3^-(I_2-F)} = C_{I_2Br^-(I_2-F)} = 0, C_{I^{\cdot}} = 100 \text{ mM},$$

$$C_{Br^-(I_2-F)} = \frac{1}{2} C_{I^{\cdot}}, D_{I^{\cdot}} = D_{I^-(I_2-F)} = D_{I_3^-(I_2-F)} = D_{I_2Br^-(I_2-F)} = 1.47 \times 10^{-5},$$

$$D_{I_2(aq)} = 1.72 \times 10^{-5}, D_{I_2(I_2-F)} = 3.00 \times 10^{-8}, D_{Br^-(I_2-F)} = 1.35 \times 10^{-5} \text{ cm s}^{-1}$$

Table S3. ED at a specific PD from the electrochemical capacitors operated in an aqueous solution with various redox active species.

Redox active species in ECs (Abbreviation if necessary)	Energy density (ED) at power density (PD)	No. of Ref. in the article
NaI + NaBr	26.2 Wh kg⁻¹ at 327.1 W kg⁻¹, 15.9 Wh kg⁻¹ at 6513.6 W kg⁻¹	This work
KSeCN	11.7 Wh kg ⁻¹ at 368.2 W kg ⁻¹ , 3.6 Wh kg ⁻¹ at 3327 W kg ⁻¹	[48]
H ₃ PW ₁₂ O ₄₀	1.6 Wh kg ⁻¹ at 98.4 W kg ⁻¹	[49]
Hydroquinone (HQ)	2.5 Wh kg ⁻¹ at 99.4 W kg ⁻¹	[49]
2, 6-Dihydroxyanthraquinone (2, 6-DHAQ)	8.9 Wh kg ⁻¹ at 119 W kg ⁻¹	[50]
K ₃ [Fe(CN) ₆]	11.8 Wh kg ⁻¹ at 188 W kg ⁻¹	[50]
K ₃ [Fe(CN) ₆]	36.9 Wh kg ⁻¹ at 225 W kg ⁻¹	[51]
Dihydroxyanthraquinone+hydroquinone (DHAQ + HQ)	21.1 Wh kg ⁻¹ at 500 W kg ⁻¹	[52]
KI	11.56 Wh kg ⁻¹ at 1000 W kg ⁻¹	[53]
Anthraquinone-2-sulfonic acid sodium (AQS)	19.35 Wh kg ⁻¹ at 1000 W kg ⁻¹	[53]

Abbreviations

Aqua-ESSs: aqueous energy storage systems

ZPI-RFB: Zn-polyiodide redox flow battery

ZIRB: Zn-iodine rechargeable battery

I-EC: Iodide redox electrolyte electrochemical capacitor

PG: pyrolytic graphite

micro-c: microporous carbon

I₂-F: Iodine-Film

η : overpotential

E_{eq} : equilibrium potential

K_{stab} : stability constant

K_{eq} : equilibrium constant

E° : standard reduction potential

C : concentration

R : gas constant

T : absolute temperature

F : Faraday constant

n_{e^-} : number of electrons

$Q_{ox \text{ or Red}}$: quantitative charge from the voltammetric oxidation and reduction peaks

E_+ : half-potential of a positive electrode

E_- : half-potential of a negative electrode

E_{cell} : cell potential

E_{oc} : open-circuit potential

SC_{cell} : specific cell capacitance

C_{ZIRB} : specific capacity of ZIRB

ED: energy density

PD: power density

References

- [1] H. Wang, H. Yi, C. Zhu, X. Wang, H. Jin Fan, *Nano Energy* 2015, **13**, 658-669.
- [2] M. Meller, J. Menzel, K. Fic, D. Gastol, E. Frackowiak, *Solid State Ionics* 2014, **265**, 61-67.